

CEAS Space Journal

Ka-band to L-band frequency down-conversion based on III-V-on-silicon photonic integrated circuits --Manuscript Draft--

Manuscript Number:			
Full Title:	Ka-band to L-band frequency down-conversion based on III-V-on-silicon photonic integrated circuits		
Article Type:	Original Article		
Corresponding Author:	Kasper Simone Van Gasse, Master of Science Universiteit Gent BELGIUM		
Corresponding Author Secondary Information:			
Corresponding Author's Institution:	Universiteit Gent		
Corresponding Author's Secondary Institution:			
First Author:	Kasper Simone Van Gasse, Master of Science		
First Author Secondary Information:			
Order of Authors:	Kasper Simone Van Gasse, Master of Science Zhechao Wang Sara Uvin Bert De Deckere Jules Mariën Lieven Thomassen Gunther Roelkens		
Order of Authors Secondary Information:			
Funding Information:	<table border="1"> <tr> <td>European space agency (ESA ARTES 5.1 'Electro-photoninc frequency converter' project.)</td> <td>Mr. Kasper Simone Van Gasse</td> </tr> </table>	European space agency (ESA ARTES 5.1 'Electro-photoninc frequency converter' project.)	Mr. Kasper Simone Van Gasse
European space agency (ESA ARTES 5.1 'Electro-photoninc frequency converter' project.)	Mr. Kasper Simone Van Gasse		
Abstract:	In this work we present the design, simulation and characterization of a frequency down-converter based on III-V-on-silicon photonic integrated circuit technology. We first demonstrate the concept using commercial discrete components, after which we turn to the use of photonic integrated devices. In the demonstrations five channels in the Ka-band (27.5 GHz to 30 GHz) with 500 MHz bandwidth are down-converted to the L-band (1.5 GHz). The breadboard demonstration shows a conversion efficiency of -20 dB and a flat response over the 500 MHz bandwidth. The simulation of a fully integrated circuit indicates that a conversion gain can be obtained on a millimeter-sized photonic integrated circuit.		
Suggested Reviewers:	<p>David Marpaung, PhD Senior Research fellow david.marpaung@sydney.edu.au Dr. Marpaung is senior researcher with expert knowledge on the field of microwave photonics.</p> <p>Guillermo Carpintero Associate professor guiller@ing.uc3m.es Professor Carpintero is a researcher with expert knowledge on microwave photonics</p>		

[Click here to view linked References](#)

Ka-band to L-band frequency down-conversion based on III-V-on-silicon photonic integrated circuits

K. Van Gasse^{1,2*}, Z. Wang^{1,2**}, S. Uvin^{1,2}, B. De Deckere^{1,3}, J. Mariën³, L. Thomassen³, G. Roelkens^{1,2}

¹Photonics Research Group, INTEC-department, Ghent University-IMEC, Belgium.

²Center for Nano- and Biophotonics, Ghent University, Belgium

³Antwerp Space, Berkenrodelei 33, 2260 Hoboken, Belgium

*kasper.vangasse@ugent.be, **zhechao.wang@ugent.be

Abstract

In this work we present the design, simulation and characterization of a frequency down-converter based on III-V-on-silicon photonic integrated circuit technology. We first demonstrate the concept using commercial discrete components, after which we turn to the use of photonic integrated devices. In the demonstrations five channels in the Ka-band (27.5 GHz to 30 GHz) with 500 MHz bandwidth are down-converted to the L-band (1.5 GHz). The breadboard demonstration shows a conversion efficiency of -20 dB and a flat response over the 500 MHz bandwidth. The simulation of a fully integrated circuit indicates that a conversion gain can be obtained on a millimeter-sized photonic integrated circuit.

Keywords

Microwave engineering, integrated photonics, frequency conversion, mode-locked laser

Aknowledgements

This work was supported by the ESA ARTES 5.1 'Electro-photoninc frequency converter' project.

1. Introduction

Frequency conversion is an important aspect of wireless communication, even more so in satellites, where signals are received and transmitted in many different frequency bands. Frequency converters based on high-speed electronics are a mature technology and offer great performance. However this approach suffers from some inherent drawbacks, such as sensitivity to EM interference and limited bandwidth. Furthermore current electronics based solutions are bulky, heavy and expensive.

An interesting alternative to the classical approach is the use of microwave photonics, a technology that brings together both the worlds of microwave engineering and opto-electronics [1]. A lot of research within the community has been dedicated to microwave photonic frequency conversion [2-4]. The basic concept of a microwave photonic frequency converter is to imprint the RF input signal on an optical carrier using an optical modulator, such as a Mach-Zehnder Modulator (MZM). The RF signal can then be mixed with a local oscillator (LO) in the optical domain, after which it is converted back to an electrical output signal using a photodiode [5]. Because the mixing happens in the optical domain, the LO generation can be centralized and then distributed using fiber, greatly reducing size and weight of the system, which is of key importance for communication satellites. Such systems can be implemented using photonic integrated circuits, providing further size and weight reduction and increasing the system reliability. This implies that in this case the LO generation can also be localized (i.e. generated close to the mixer for every individual microwave photonic mixer) without substantially impacting the system mass-power-volume envelope. A promising photonic integration technology is the hybrid III-V-on-Silicon platform, which combines passive Si photonic waveguide circuits with III-V lasers, high-speed modulators and photodiodes. Using this technology the entire system can be put on one compact photonic integrated circuit (PIC) to create a fully integrated Electronic-Photonic Frequency Converter (EPFC).

In this paper we elaborate on the design, simulation and characterization of an EPFC. In the second section of the paper the system design of the EPFC is explained in detail. In the third section a breadboard demonstration of the EPFC system is shown. In the fourth section a detailed explanation of the design and fabrication of the integrated photonic components is given, together with a down-conversion experiment using individual PICs. The obtained results are compared with simulations, and the system performance of a fully integrated circuit is assessed in section 6.

2. System design

The system architecture is shown in Fig. 1. The first key element of the EPFC system is a mode-locked laser (MLL). This laser creates an optical pulse train with a fixed repetition rate and picosecond pulse width. The second component is a Mach-Zehnder modulator with phase shifters that can be independently driven, commonly referred to as a Dual-Drive Mach-Zehnder Modulator (DD-MZM). The third component is a photodiode with sufficient power handling and bandwidth. Optical amplifiers can be used to increase the conversion efficiency of the system.

The basic operation principle is as follows. The RF signal to be down-converted drives one arm of the DD-MZM while a LO signal drives the other [6]. The optical pulse train generated by the mode-locked laser samples both signals and mixes them on the photodiode. In Fig. 1 an input RF signal with a frequency of 29.25 GHz (Ka-band) is down-converted to an IF of 1.5 GHz (L-band). The repetition rate of the mode-locked laser is chosen together with the frequency of the LO to achieve the wanted IF frequency, in this case 15.95 GHz and 4.15 GHz respectively. The optical output spectrum of the mode-locked laser can be represented as an optical frequency comb separated by the repetition rate of the MLL, as shown in Fig.1 (1). When phase modulated in top and bottom arm every line of the frequency comb will develop side bands, separated from the carrier by the RF and LO frequency respectively, as shown in Fig. 1(2). In one of the arms of the DD-MZM a static π -phase shift is applied, such that when both signals are combined the carriers are cancelled. This results in the case of ideal suppression of the carriers, in an optical spectrum shown in Fig. 1(4). When this signal is incident on the photodetector, the beating of the different lines

creates different RF signals, of which one is the wanted IF output. Because the output of the photodiode produces several beat notes a bandpass filter is needed to isolate the IF.

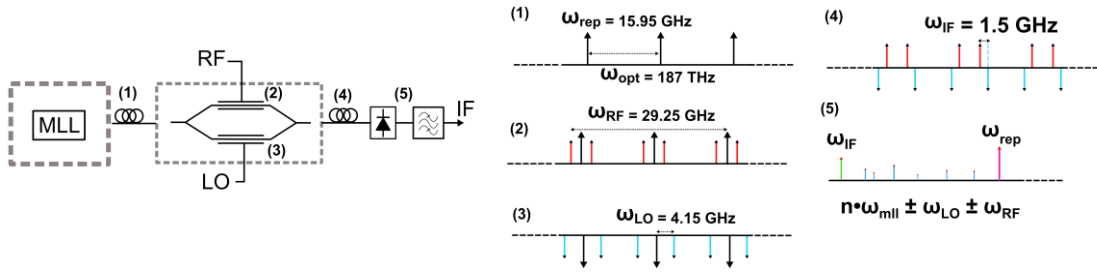


Fig. 1. Overview of the EPFC system. (1) optical spectrum of the MLL output. (2) optical spectrum after RF phase modulation. (3) optical spectrum after LO phase modulation. (4) optical spectrum obtained after combining the output of both phase shifters. (5) electrical spectrum obtained at the output of the photodiode before the bandpass filter.

All the generated beat notes can be written as a combination of the MLL repetition rate, the RF and LO frequency:

$$f_{if} = k \cdot f_{rep} - l \cdot f_{LO} - m \cdot f_{RF} \quad k, l, m \in \mathbb{Z}$$

The wanted IF frequency in our chosen frequency plan is created by the beat note

$$f_{if} = 2 \cdot f_{rep} - f_{LO} - f_{RF}$$

This very versatile approach allows down-converting any given input frequency to any wanted intermediate frequency, the only limiting factor being the bandwidth of the modulator and photodetector. Upconversion can be realized as well. The MLL repetition rate and LO frequency are chosen in such a way that beat note is created at a chosen IF. In the remainder of this paper we will focus on the downconversion of five channels in the Ka-band with a bandwidth of 500 MHz at center frequencies 27.75, 28.25, 28.75, 29.25 and 29.75GHz. The MLL repetition rate was chosen at 15.95 GHz, together with the LO frequencies 5.65, 5.15, 4.65, 4.15, 3.65 GHz. This frequency plan allows all channels to be down-converted to an IF of 1.5 GHz without creating any spurious beat note in a 500 MHz band. This system has the benefit that a different channel can be chosen by changing the LO frequency instead of the MLL repetition rate, which allows working with a single mode-locked laser source.

3. Breadboard demonstration

As a first validation of the EPFC system, a breadboard demonstration was performed with commercial table-top equipment. An overview of the measurement set-up is shown in Fig. 2. As optical source a Calmar pico-second MLL was used with a pulse width of 3 picoseconds and a repetition rate of 10.3 GHz. Because the repetition rate of the MLL could not be tuned to the wanted 15.95 GHz, the frequency scheme was changed to:

$$f_{if} = 3f_{rep} - f_{LO} - f_{RF}$$

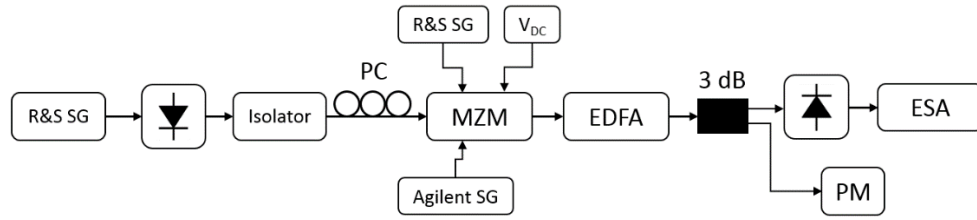


Fig. 2. Overview of the measurement set-up used for the breadboard demonstration of the EPFC system.

The MLL repetition rate was locked to the output of a Rhode&Schwarz RF signal generator. The output of the laser was sent through an optical isolator and polarization controller, after which it is coupled into a Fujitsu FTM7937EZ LiNbO₃ dual-drive MZM. The modulator was biased at the minimum transmission point. The phase shifters of the modulator were driven by the input RF signal and the LO signal. The LO signal was fixed at -1 dBm and a frequency of 4.15 GHz. The RF power of the input signal was fixed at -10 dBm and a frequency of 28.25 GHz, corresponding to the second Ka-band channel. At the output of the MZM an EDFA with automatic gain control was placed with a fixed output power of 0 dBm. The photodiode was a Discovery Semiconductor DSC10 with 40 GHz bandwidth and 0.5 A/W responsivity. The output of the photodiode was analyzed with an Agilent Electrical Spectrum Analyzer (ESA) with 44 GHz bandwidth. The RF spectrum obtained at the output of the photodiode is shown in Fig. 3(left). A clear signal was observed at 1.5 GHz with a power of -30 dBm, which means that the total system has a conversion efficiency of -20 dB. No electrical amplification was used after the photodiode. Fig. 3 (right) shows a zoom-in of the IF band, when sweeping the RF input signal over a 800 MHz span around the channel center frequency of 28.25 GHz (-20 dBm RF input power). It can be seen that the response shows no more than 1.5 dB ripple. The ripple is caused by the non-flat response of the DD-MZM and can be easily equalized. The experiment was repeated for all five channels by changing the LO frequency in steps of 500 MHz, showing similar results.

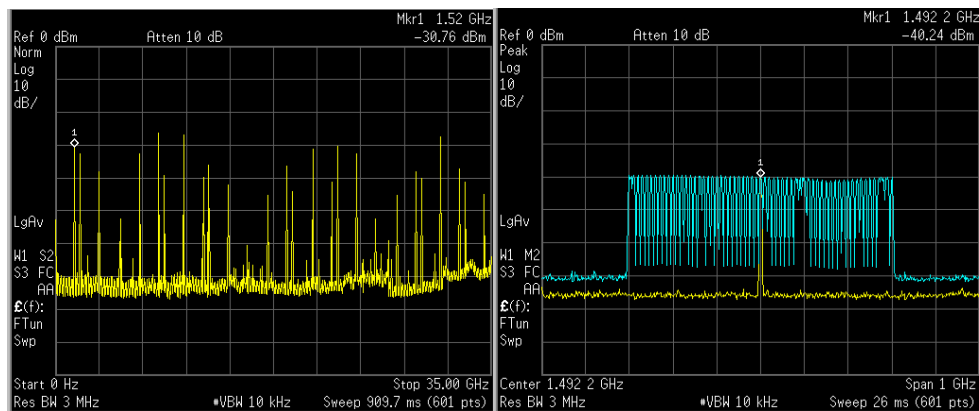


Fig. 3. (Left) Electrical output spectrum after the photodiode from 0 to 35 GHz. (Right) IF output of Channel 2 swept 800 MHz in frequency for an RF input signal of -20 dBm.

4. III-V-on-silicon integrated opto-electronic components for the EPFC

While this breadboard demonstration shows that the concept of an electronic-photonics frequency converter is sound, the real benefit from using a microwave photonics approach to down-conversion is the possibility to substantially reduce size, weight and power consumption by miniaturizing the system to a single chip. In this work we use a III-V-on-silicon integration platform, in which the passive waveguide circuits are implemented in a silicon-on-insulator waveguide layer and the active opto-electronic components are realized in a III-V waveguide layer, adhesively bonded on top. A more detailed description of the III-V integration process and post-processing of the

III-V opto-electronic components can be found in [7]. Here we describe the key components to be implemented on this integration platform for the EPFC: the III-V-on-silicon mode-locked laser and the Mach-Zehnder modulator.

4.1 III-V-on-silicon mode-locked laser

A schematic layout of the MLL is shown in Fig. 4 (left). The devices are implemented on a silicon-on-insulator wafer with 400 nm Si device layer thickness, etched 180 nm to define the waveguide structures. The MLL consists of a passive waveguide section with at one end a high reflectivity grating (DBR, distributed Bragg reflector) and on the other end the III-V waveguide section. The III-V layer structure consists a p-doped InGaAs contact layer, a p-doped InP cladding, a InGaAsP MQW active waveguide, consisting of 6 quantum wells with a photoluminescence peak around 1.55 μm , and a n-doped InP contact layer. The III-V waveguide section consists of a tapered InP and Si waveguide followed by a III-V waveguide amplifier (SOA) and a saturable absorber (SA) with a Si grating reflector (DBR) underneath. The SA is electrically isolated from the gain section by etching slits into the p-doped III-V contact layer. After the SA an amplifying taper structure is placed which couples the light into the Si waveguide. At the end of the waveguide there is a vertical grating coupler to couple the light into a single mode fiber. As the saturable absorber is placed at the output coupler of the laser, this structure is an anti-colliding pulse configuration MLL. Such a design was adopted because of high optical output power and short optical pulses that can be generated this way [8]. In Fig. 4 (right) an electrical spectrum is shown, generated by the MLL pulses incident on a high bandwidth PD. From the spectrum we can clearly see that the laser generates a pure beat note at 15.584 GHz and the 31.168 GHz, corresponding to the repetition rate of the mode-locked laser and the first harmonic. A more detailed description of the operation principle and performance of this type of mode-locked lasers can be found in [9].

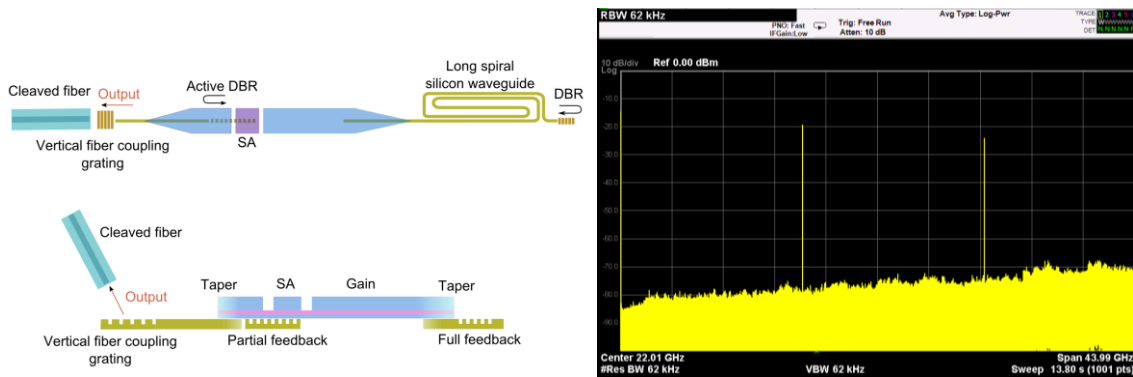


Fig. 4. (Left) Schematic top view and side view of the integrated MLL. (Right) RF output spectrum generated by the MLL.

4.2 Integrated Mach-Zehnder modulator

A second main component for the integrated EPFC is the MZM, which was also realized on the III-V-on-Silicon waveguide platform. In Fig. 5. a schematic and microscope image of the MZM is shown. The Mach-Zehnder interferometer structure is realized in the Si waveguide layer, while the phase shifters are realized in the bonded III-V material. The optical input and output of the MZM are provided by 2X2 multimode interferometers (MMIs) acting as 3dB power splitters/combiners. The III-V layer stack used for this component consists of a p-doped InP cladding with InGaAs contact layer, a AlGaInAs MQW region, consisting of 15 quantum wells with a photoluminescence peak at 1.36 μm and a n-doped InP contact layer. This layer structure, with a bandgap to wavelength offset of 190 nm allows for the efficient phase modulation of the optical pulses generated by the MLL. A similar tapering from Si to III-V waveguide was used for the phase sections. As can be seen in Fig. 5 the phase shifters are driven by segmented travelling wave electrodes, designed for high bandwidth operation of the MZM. An additional thermo-optic heater is fabricated in the bottom arm to provide a static π phase shift. There are bond pads foreseen to enable probing or wire bonding on one side and termination on the other. The phase shifting section is 1.5 mm long and has a static V_{π} of 2.1 Volt, resulting in a modulator $V_{\pi}L_{\pi}$ of 3.15 Vmm, and an insertion loss of 7dB. A static

measurement of the MZM transmission when changing the bias of the top phase shifter is shown in Fig. 6 (left). The small-signal frequency response to determine the bandwidth of the phase shifters is shown in Fig. 6 (right).

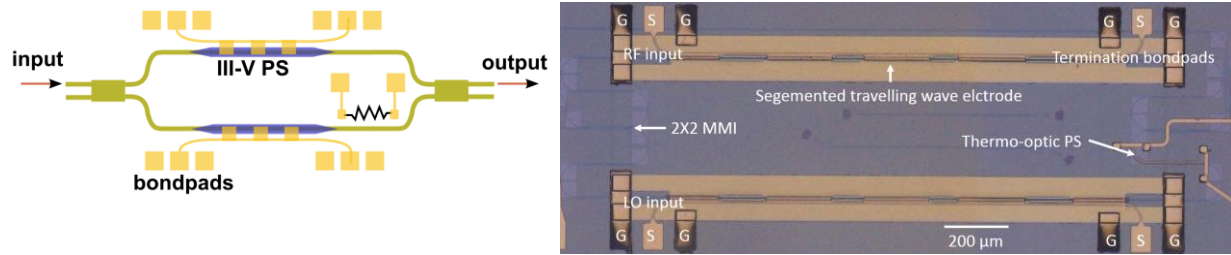


Fig. 5. (Left) Schematic of the III-V-on-silicon MZM; (Right) Microscope image of the realized III-V-on-Silicon MZM with the separate components indicated.

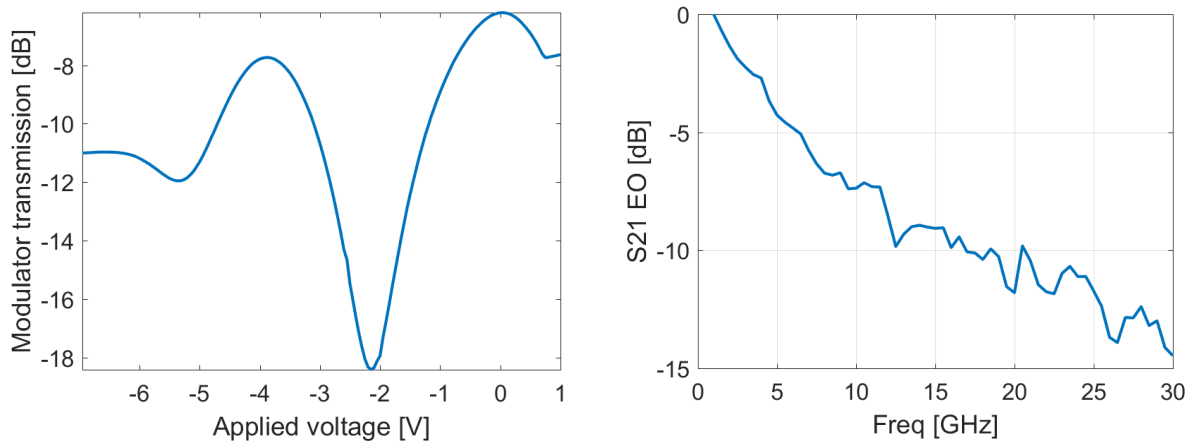


Fig. 6. (Left) Static characterization of the III-V-on-Si MZM indicating a V_{π} of 2.1V and an insertion loss of 7 dB. (Right) Small signal frequency response of the modulator when one arm is driven.

5. Demonstration of the EPFC with individual III-V-on-silicon components

An EPFC system was built with a III-V-on-silicon MLL chip and a III-V-on-silicon MZM chip. The layout of the measurement set-up is shown in Fig. 7. The MLL PIC was placed on a temperature-controlled stage and was kept at 20°C. To lock the repetition rate of the laser to 15.584 GHz an Anritsu Signal generator was used. A cleaved SMF was used to collect the light from the laser through a fiber-to-chip grating coupler. The on-chip output of the MLL is approximately 2 mW, the fiber-to-chip grating couplers however have approximately 10 dB loss. Therefore, an EDFA between the laser and MZM PIC is used to compensate for these losses. The light is then coupled into the MZM PIC, also using a cleaved SMF and fiber-to-chip grating couplers. The two independent phase shifters of the MZM are driven by the LO and the RF input signal. Due to experimental limitations, we were unable to use the heater to bias the MZM. Therefore the phase shifters were DC-biased differently for minimum transmission of the MZM. Because the grating couplers of the MZM PIC also have 10 dB loss an additional EDFA was placed at the output. A Santec optical tunable filter (OTF-350) was placed after the EDFA to filter out the excess noise. The average optical power incident on the PD was 0 dBm. To boost the electrical output signal a photodetector with Trans-Impedance Amplifier (TIA) was used. The receiver has a gain of 150 V/W.

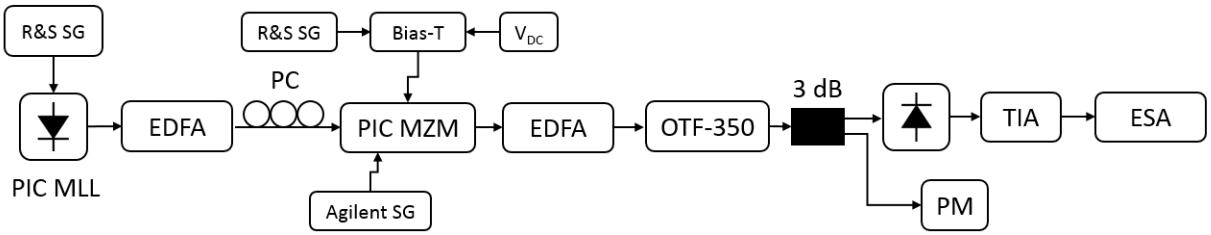


Fig. 7. Overview of the measurement set-up for PIC based EPFC demonstration.

In the experiment all five Ka-band channels were successfully down-converted to an IF of 1.5 GHz. Fig. 8 (left) shows the first down-converted channels where the input was swept over 700 MHz. Again a flat frequency response is obtained. To further analyze these results a simulation of the system was performed using VPI software [10]. In Fig. 8 (right) the electrical output spectrum for Channel 2 from the measurement is shown in blue. The simulated spectrum is overlapped in the same graph. Excellent agreement between simulation and measurement is found. For the simulation mode-locked laser pulses with a FWHM of 3 ps are assumed, as was measured for an identical device with different repetition rate [9]. The EDFAs were modeled using the standard VPI model.

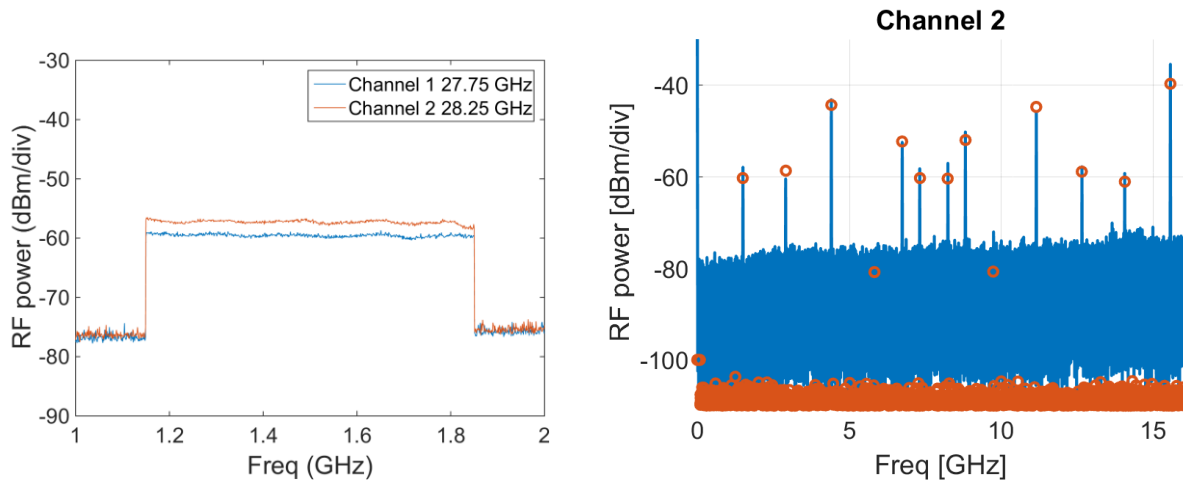


Fig. 8. (Left) IF output of Channel 1 and 2 swept over 700 MHz around the center frequency. (Right) Full RF output spectrum in blue with IF at 1.5 GHz. The orange dots represent the weight of the different RF tones of the simulated RF spectrum. A good match between theory and experiment is obtained.

6. Towards a fully integrated EPFC

Now that we demonstrated that the EPFC can be realized using miniaturized photonic devices, the final goal is to bring all the components together on one photonic integrated circuit. In Fig. 9 one can find a schematic of what a fully integrated device would look like. The full PIC would be realized in III-V-on-Silicon where the MLL gain section, SOA and PD would all be realized in the same aforementioned III-V epitaxial layer structure. The MZM would be realized in a different aforementioned layer stack. The bonding of different III-V materials on the same passive Si PIC has been demonstrated before [11]. After PIC processing, the PIC would be placed on a PCB to create a RF and LO input port, as well as an input for the MLL reference to lock the repetition rate. Termination for the MZM would also be foreseen on the PCB, strongly improving modulation efficiency. An LNA would be placed on the PCB to amplify the weak RF input signal before feeding it to the Mach-Zehnder modulator. To determine the performance of this system a VPI simulation was performed. The parameters for the MLL and MZM are based on the model used for the PIC system. The on-chip SOA is modeled based on measurement results of already fabricated and tested III-

V-on-Si SOAs [7]. The LNA (type CGY2128UH/C1) was modeled using the standard VPI model and the specs of the data sheet. The simulated spectrum at the output of the photodiode, before the IF bandpass filter, for an RF input power of -20 dBm (for the first channel) and an LO input power of -1 dBm is shown in Fig. 10 (left). The conversion efficiency of the full system is -4 dB. However the conversion efficiency is tunable by changing the LO input power as is shown in Fig. 4. (right). For an input power larger than 4 dBm conversion gain is achieved.

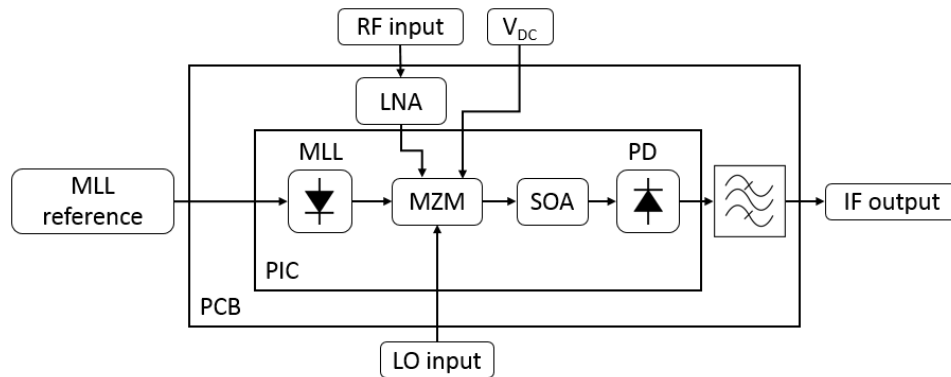


Fig. 9. Schematic of the fully integrated EPFC.

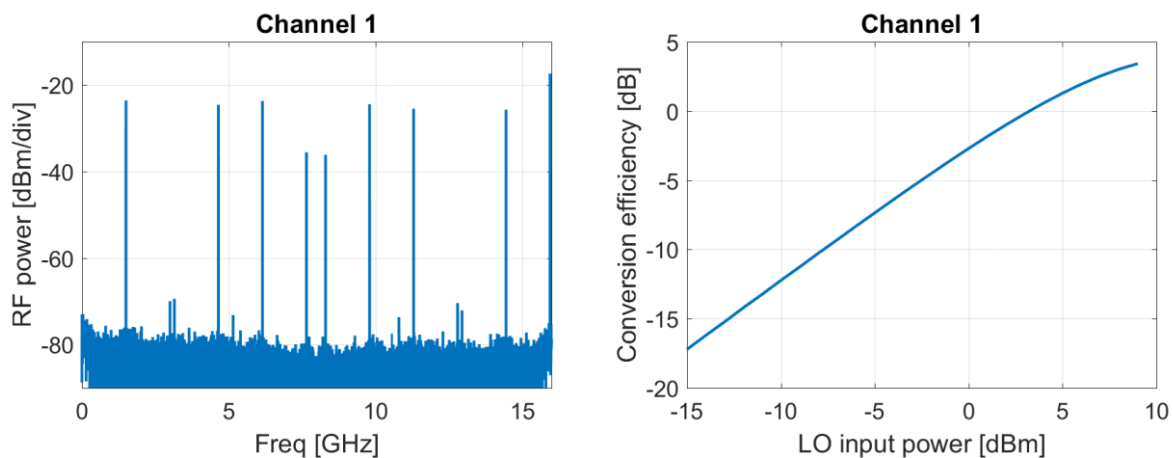


Fig. 10. (Left) Simulated spectrum for down-conversion of channel 1. (Right) Conversion efficiency as function of the LO input power for a RF input power of -20 dBm (before LNA).

7. Conclusion

In this work we have shown the design of a fully integrated Electro-Photonic Frequency Converter. We demonstrated the operation principle with both a breadboard system and a PIC based system. Using the results of the PIC based demonstration a model for a device including all optical components on one III-V-on-Si PIC was developed. The simulated EPFC showed conversion gain when an LNA is included in the system. These encouraging results lead us to the realization of a fully integrated III-V-on-silicon EPFC chip, the fabrication of which is currently ongoing.

References

[1] Marpaung D., Roeloffzen C., Heideman R., Leinse A., Sales S., Capmany J.: Integrated microwave photonics. *Laser & Photonics Reviews*, 7(4), 506-538 (2013)

- 1
2
3
4 [2] Cabon B., Le Guennec Y., Lourdiane M., Maury G.: Photonicmixing in RF modulated optical links. Proc.
5 IEEE 19th Annu. Meeting Lasers and Electro-Opt. Soc., 408–409 (2006)
6
7 [3] Zhang T., Zhang F., Chen X., Pan S.: A simple microwave photonic downconverter with high
8 conversion efficiency based on a polarization modulator. Asia Communications Photonics Conf.,
9 Shanghai, China, Paper AF2E.4. (2014)
10
11 [4] Guennec Y. L., G. Maury, J. Yao, Cabon B.: New optical microwave up-conversion solution in radio-
12 over-fiber networks for 60-GHz wireless applications. J. Lightw. Technol., vol. 24, no. 3, 1277–1282
13 (2006)
14
15 [5] Yao J.: Microwave Photonics. J. Lightw. Technol., vol. 27, no. 3, 314-335 (2009)
16
17 [6] Chan E. H., Minasian R. A.: Microwave Photonic Downconverter With High Conversion Efficiency. J.
18 Lightw. Technol., vol. 30, no. 23, 3580-3585 (2012)
19
20 [7] Roelkens G. et al.: III-V-on-silicon photonic devices for optical communication and sensing. Photonics
21 (invited), 2(3), 969-1004 (2015)
22
23 [8] Zhuang J.P., Pusino V., Ding Y., Chan S.C., Sorel M.: Experimental investigation of anti-colliding pulse
24 mode-locked semiconductor lasers. Optics letters, 40(4), 617-620 (2015)
25
26 [9] Keyvaninia S. et al.: Narrow-linewidth short-pulse III-V-on-silicon mode-locked lasers based on a
27 linear and ring cavity geometry. Optics Express, 23(3), 3221-3229 (2015)
28
29 [10] VPI-Photonics design automation
30
31 [11] Hulme J. C. et al.: Fully integrated heterodyne microwave generation on heterogeneous silicon-
32 III/V. 2016 IEEE International Topical Meeting on Microwave Photonics (MWP), Long Beach, CA, 336-339
33 (2016)
34
35
36
37
38
39
40
41
42
43
44
45
46
47
48
49
50
51
52
53
54
55
56
57
58
59
60
61
62
63
64
65